Adaptive Monitoring of Mobile Robot

R. Merzouki, K. Fawaz, B. Ould Bouamama
LAGIS, UMR CNRS 8146, Ecole Polytechnique de Lille,
Avenue Paul Langevin,
59655 Villeneuve d'Ascq, France.
Rochdi.Merzouki@polytech-lille.fr

May 16, 2008

Abstract

This paper deals with a model-based fault detection and isolation (FDI) approach in order to detect and to isolate the transmission channel fault from the actuators faults of a mobile robot. A dynamic model of the robot system is developped and it includes the transmission channel dynamic. A Co-simulation with a virtual robot is proposed, in order to show the faults influences on the synthesized residuals. Simulation and experimental results show clearly the isolability between the studied faults.

1. Introduction

Modern mechatronics systems are more and more intelligent due to their ability to control, supervise and maintenance all internal components. More and more that the controlled systems are taken a certain autonomy of operation, then they should be perfectly supervised and maintained at distance via a transmission channel. Many works have been done on the distributed control systems during the last decade as in [12], where a Takagi–Sugeno (T–S) model is used to represent a networked control system (NCS) with different network-induced delays. Comparing with existing NCS modelling methods, this approach addresses situations involving all possible network-induced delays. Moreover, this approach also handles data-packet loss. For the FDI problematic, a parity-equation approach

and a fuzzy-observer-based approach for fault detection of an NCS are developed. Then, Kalman filters are constructed for NCS in [13] according to different system faults. In [7], the parity-equation approach and the observer-based approach are used for residual generation. In [14], the introduction of the so-called stationary wavelet transform into the residual signal for residual generator, shows a new approach which ensures a good performance index, a satisfactory low misdetection rate and a suitable response speed to faults with a low order parity vector and a simple online implementation form. Among some results related to diagnosis of actuators faults, in [8], a contribution on how to detect and to localize the failures introduced by the mechanical backlash is proposed. The main purpose is to distinguish the disturbing backlash from the useful one during a normal operation of the electromechanical system, while in [2], the residuals and the thresholds are generated in presence of parameter uncertainties, using bond graph representation under linear fractional transformation form (LFT), and applied for a mechatronic system. The whole of : nonlinear system model, structural analysis, residual with adaptive thresholds generations, and residual sensitivity analysis, are synthesized using the bond graph properties.

In this paper, a dynamic model of a mobile robot with the transmission channel is developed and validated experimentally. For modelling such systems, one needs an unified approach as Bond graph tool [5], [6], to represent the multiphysical aspect and to exploit the structural and causality properties for generating the diagnostic algorithm [1]. Then, a co-simulation model based between a virtual and a real mobile robot is presented. It concerns the on line telediagnosis of transmission channel and actuators faults of a mobile robot.

Two innovative points are given through this work: the first concerns the transmission channel which is considered as a uncoupled system, modelled separately from the robot model, and concatenated to this latter for the FDI algorithm synthesis. The second point relates to the development of a virtual simulator based on the dynamic robot system' model, which can work in parallel with the real robot. The interest of this simulator is its ability to inform the system supervisor of any transmission and/or actuators faults, without being closer to the real system.

This paper is organized as follows: after the introduction section, a modelling step of the set of the transmission channel and the mobile robot is given in Section 1. Section 2 presents the Fault Detection and Isolation (FDI) algorithm. Section 3 is devoted to simulation and experimental results done on the mobile robot system.

2. Dynamic model of global system

In this section, a description of the principal studied system parts is introduced. Also, the modelling of the transmission channel and the miniature mobile robot is presented.

2.1. Robot System Description

The studied mobile robot $Khepera\ II$ [3], is a double active wheeled and miniature robot (Fig. 1-(a)).

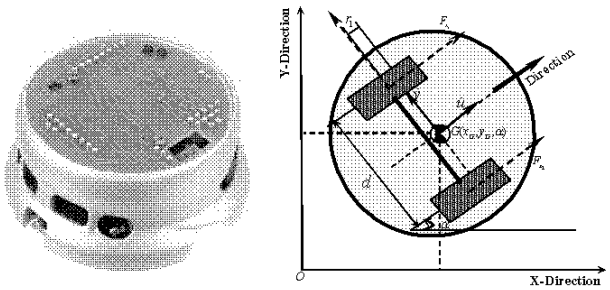

Figure 1: (a): Khepera II robot - (b): Robot description schema

Each wheel is moved by a DC motor coupled with the wheel through a $25:1$ reduction gearbox. An incremental encoder, placed on the motor axis, gives 24 pulses per revolution of the motor. This allows a resolution of 600 pulses per revolution of the wheel that corresponds to 12 pulses per millimeter of path of the robot. The motor controller can be used in two control modes: The velocity and the position modes. The active control mode is set according to the kind of command received. If the controller receives a velocity control command, it switches to the velocity mode. If the controller receives a position control command, the control mode is automatically switched to the position mode. Different PID control parameters (Kp, Ki and Kd) can be set for each of the two control modes.

2.2. Robot modelling hypothesis

Some hypothesis are taken in consideration for these part according to the robot characteristics and its environment:

1. The contact area between robot wheels and the motion surface is assimilated to a point contact, due to the rigidity of the wheel tire;

2. The contact efforts are considered static in function of the time, due to the homogeneous of the contact area. They are taken as a system inputs;

3. For the miniature robot actuators, only the electrical and mechanical dynamics are considered;

4. For dynamic robot modelling, only longitudinal and yaw dynamics are studied. The lateral dynamic is neglected due to the minor lateral efforts on the robot dynamic motion, issued from a so small width of the wheels' contact.

2.3. Word Bond Graph

The word bond graph represents the technological level of the model where the global system is decomposed into four principle subsystems (Fig. (2)): the cable part, the j^{th} electromechanical part with the j^{th} wheel, the longitudinal and the yaw parts. Comparing to classical block diagram, the input and output of each subsystems define a power variables represented by a conjugated pair of effort-flow represented by a half arrow. Power variables used for the studied system are:

$$(Torque, Angular\ velocity) = \left\{(C_j, \dot{\theta}_{e_j}), (F_{x_1}.R, \dot{\theta}_{s_1}), (F_{x_2}.R, \dot{\theta}_{s_2})\right\};$$
$$(Voltage, current) = \left\{(U_{in}, i_{in}), (U_s, i_s), (U_{0_j}, i_j)\right\}.$$

F_{x_j} is the j^{th} traction contact efforts, R is the robot wheel radius, $\dot{\theta}_{s_j}$ is the j^{th} wheel angular velocity, $(C_j, \dot{\theta}_{e_j})$ are the transmitted torque to gears part and the input velocity for the j^{th} electromechanical system, (U_{in}, i_{in}) are the input voltage and current of the serial cable, (U_s, i_s) are the output voltage and current of the serial cable, (U_{0_j}, i_j) is the input voltage and current of the j^{th} electromechanical system.

These true and pseudo bond graph variables are associated respectively with electrical and mechanical rotation aspects.

The internal robot circuit part of Fig. (2) is not modelled in this work, due to the lack of information about this part.

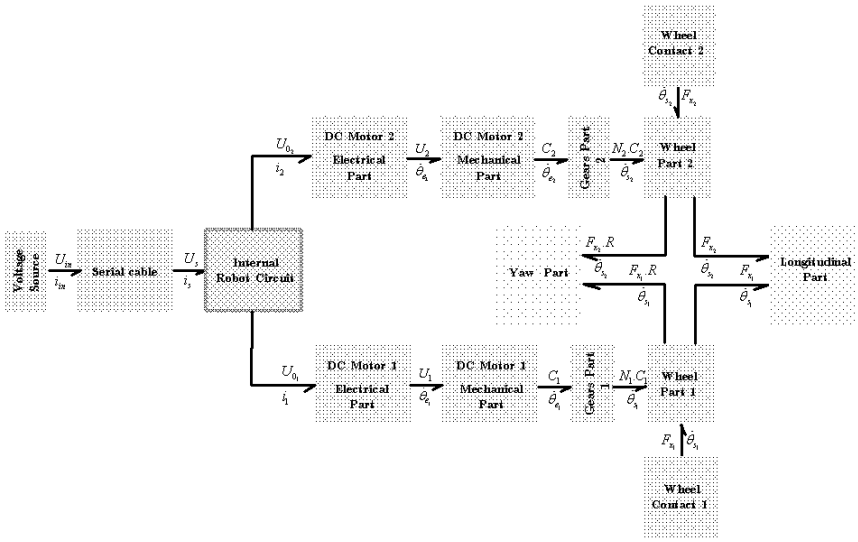

Figure 2: Word bond graph structure of the mobile robot

2.4. Electromechanical system modelling

There are two electromechanical systems located inside the robot and used for the traction motion. They are constituted by three principal components (Fig. 3): the DC motor part, which is the combination of an electrical and a mechanical parts, the gears system part and the wheel system part. In this subsection, dynamic bond graph models of all of these components are graphically synthesized then expressed by differential equations.

2.4.1. Electrical part of the DC motor

This part corresponds to RL electrical circuit of the j^{th} DC motor (Fig. 4), composed by: input voltage' source U_{0_j}, electrical resistance R_{e_j}, inductance L_j and back electromotive force EMF , which is linear to the angular velocity of the rotor $\dot{\theta}_{e_j}$and equal to $k_{e_j}.\dot{\theta}_{e_j}$ with k_{e_j} the EMF constant. The index $j \in [1, 2]$ corresponds to the j^{th} motor of the robot.

The corresponding RL circuit bond graph' model is given in integral causality by Fig. 5.

Let's note e_{1_j}, P_{1_j}, M_{1_j} , effort, momentum and algebraic value of element I

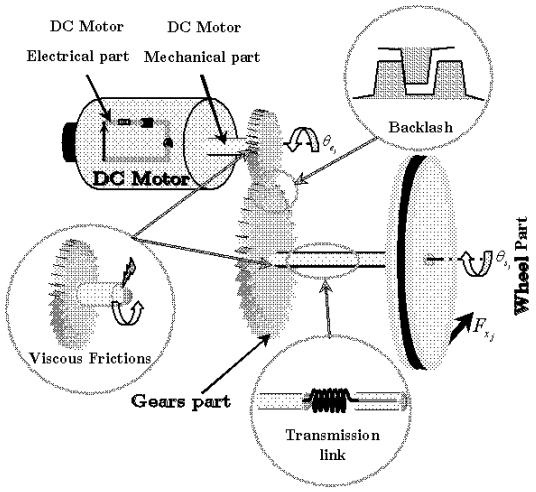

Figure 3: jth Electromechanical system' components of the mobile robot.

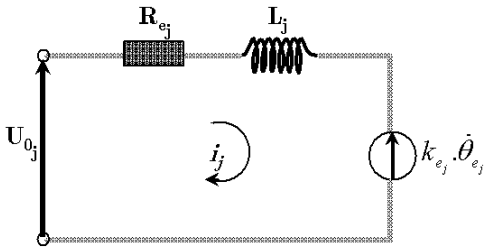

Figure 4: Electrical RL circuit of the j^{th} DC motor

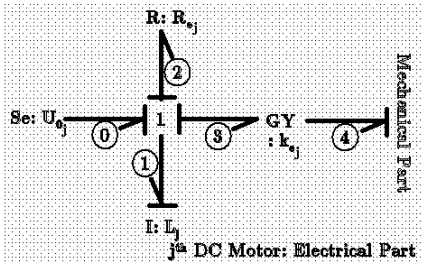

Figure 5: Bond graph model of the electrical part of the j^{th} DC motor

of the j^{th} motor (Fig. 5). The gyrator element GY describes the power transfer from the electric to mechanic by a flow variable f_{4_j} of the link 4 and Se_{0_j} is the input voltage source, then the following state equation is obtained:

$$e_{1_j} = Se_{0_j} - R_{e_j}.\frac{P_{1_j}}{M_{1_j}} - k_{e_j}.f_{4_j} \tag{1}$$

with:

$$\begin{cases} f_{0_j} = f_{1_j} = f_{2_j} = f_{3_j} = \frac{1}{L_j}.\int e_{1_j}.dt = \frac{P_{1_j}}{M_{1_j}} = i_j \\ Se_{0_j} = U_{0_j} \\ f_{4_j} = \dot{\theta}_{e_j} \end{cases}$$

Thus, the corresponding dynamic equation of circuit of Fig. 4 is:

$$L_j.\frac{di_j}{dt} = U_{0_j} - R_{e_j}.i_j - k_{e_j}.\dot{\theta}_{e_j} \tag{2}$$

2.4.2. Mechanical part of the DC motor

This part represents the mechanical part of the j^{th} DC motor, characterizing by its rotor inertia J_{e_s}, viscous friction parameter f_{e_j}, transmission axis rigidity K_j and a motorized torque U_j. In this part, the influence of backlash phenomenon expressed by a disturbing torque w_j is represented by a modulated effort source for the bond graph model [9]. The corresponding bond graph model in integral causality is given by Fig. 6.

The backlash mechanism considered in this model is represented by a disturbing torque, hampering the smooth functioning of the system, and caused by

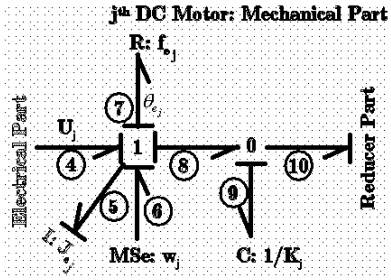

Figure 6: Bond graph model of the mechanical part of the j^{tj} DC motor

simultaneous and evaluative reactions of the shock between the two sides of the gears system (Fig. 7) . This torque is chosen continuous, nonlinear and differentiable, compared to the size of the gears system and its effect on the global system.

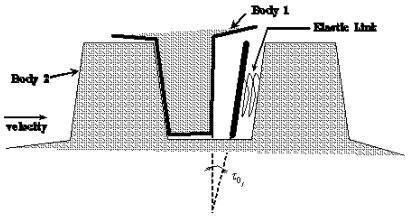

Figure 7: Backlash mechanism for the jth DC motor

So, a smooth and continuous model of transmitted torque w_j which is developed in [9] and illustrated in Fig. 7, is taken as a modulated effort source $(MSe : w_j)$ (Fig. 6). This torque is expressed as follows:

$$w_j = A_j.K_j.\tau_{0_j}.\frac{1 - e^{-\gamma_j.\Delta\theta_j}}{1 + e^{-\gamma_j.\Delta\theta_j}} \tag{3}$$

where w_j is the disturbing and nonlinear transmitted torque, $\Delta\theta_j = \theta_{e_j} - N_j.\theta_{s_j}$ defines the difference between input θ_{e_j} and output θ_{s_j} motor positions, N_j a reducer constant, A_j a graphical parameter which is taken as a negative integer to describe the reaction effect of the disturbing torque, K_j the rigidity constant

of the transmission system, τ_{0j} is the dead zone amplitude and $\gamma_j = 1/\left(2.\tau_{0_j}\right)$ the sigmoid function slope of the j^{th} DC motor [9].

Let's note e_{5_j}, P_{5_j}, M_{5_j} effort, momentum and algebraic value of element I of Fig. 6, f_{4_j} is the flow variable of link 4, f_{9_j},$1/K_j$ flow and algebraic value of element C, then the following state equation (4) is obtained:

$$e_{5_j} = -f_{e_j}.\frac{P_{5_j}}{M_{5_j}} + e_{4_j} + e_{6_j} - K_j.\int f_{9_j}.dt \tag{4}$$

with:

$$\begin{cases} f_{4_j} = f_{5_j} = f_{6_j} = f_{7_j} = f_{8_j} = \frac{1}{J_{e_j}}.\int e_{5_j}.dt = \frac{P_{5_j}}{M_{5_j}} = \dot{\theta}_{e_j} \\ e_{8_j} = e_{9_j} = K_j.\int f_{9_j}.dt \\ f_{9_j} = f_{8_j} - f_{10_j} = \dot{\theta}_{e_j} - N_j.\dot{\theta}_{s_j} \\ e_{4_j} = U_j = k_{c_j}.i_j \\ e_{6_j} = w_j \end{cases}$$

Thus, the corresponding dynamic equation of mechanical part is given as follows:

$$J_{e_j}.\frac{d\dot{\theta}_{e_j}}{dt} = -f_{e_j}.\dot{\theta}_{e_j} + U_j - w_j - K_j.\left(\theta_{e_j} - N_j.\theta_{s_j}\right) \tag{5}$$

with U_j the input motor torque of the j^{th} DC motor, given in function of the current i_j and the torque constant k_{c_j} .

2.4.3. Gears part

This part concerns the mechanical gears which links between the mechanical and the load parts with a reduction constant N_j (Fig. 3). Bond graph model of this part is given by Fig. 8 and represents a transformer element TF between the j^{th} velocities of the motor axis $\dot{\theta}_{e_j}$ and the wheel $\dot{\theta}_{s_j}$.

According to Fig. (8), let's choose f_{10_j} and f_{11_j} as the corresponding flows variables of links 10 and 11:

$$f_{10} = N_j.f_{11} \tag{6}$$

which corresponds to the mechanical equation:

$$\dot{\theta}_{e_j} = N_j.\dot{\theta}_{s_j} \tag{7}$$

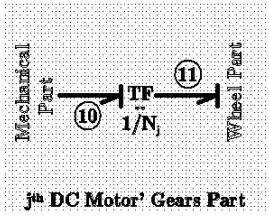

Figure 8: Bond graph model of jth gears part

2.4.4. Wheel part

This part represents the load part of the j^{th} electromechanical system, characterizing by its inertia J_{s_j}, viscous friction parameter f_{s_j} and backlash disturbing torque $N_j.w_j$. The bond graph model of this part in integral causality is given by Fig. 9.

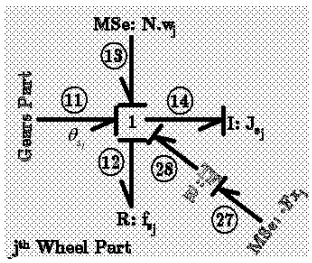

Figure 9: jth Wheel part bond graph' model

Let's note e_{14_j}, P_{14_j}, M_{14_j} effort, momentum and algebraic value of element I of Fig. 9. f_{9_j} is the flow and of element C (Fig. 6), then the following state equation (8) is obtained:

$$e_{14_j} = -f_{s_j}.\frac{P_{14_j}}{M_{14_j}} + e_{13_j} + e_{11_j} + e_{28_j} \tag{8}$$

with:

$$\begin{cases} f_{11_j} = f_{12_j} = f_{13_j} = f_{14_j} = \frac{1}{J_{s_j}}.\int e_{14_j}.dt = \frac{P_{14_j}}{M_{14_j}} = \dot{\theta}_{s_j}; \\ e_{11_j} = N_j.e_{9_j} = N_j.K_j.\int f_{9_j}.dt; \\ f_{9_j} = f_{8_j} - f_{10_j} = \dot{\theta}_{e_j} - N_j.\dot{\theta}_{s_j}; \\ e_{13_j} = N_j.w_j; \\ e_{28_j} = R.e_{27_j} = -R.F_{x_j} \end{cases}$$

Thus, the corresponding dynamic equation of mechanical part is given as follows:

$$J_{s_j}.\frac{d\dot{\theta}_{s_j}}{dt} = -f_{s_j}.\dot{\theta}_{s_j} + N_j.w_j + N_j.K_j.\left(\theta_{e_j} - N_j.\theta_{s_j}\right) - R.F_{x_j} \tag{9}$$

F_{x_j} are the contact efforts which are the origin of the longitudinal an yaw dynamics.

After a concatenation of the different bond graph models, the global model of the j^{th} electromechanical system is deduced in Fig. 10. The measured states are shown by detectors element $Df : \dot{\theta}_{e_j}$ and $Df : \dot{\theta}_{s_j}$.

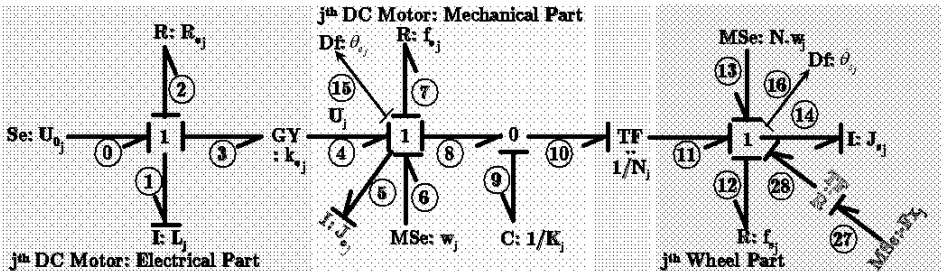

Figure 10: jth Global bond graph model of the electromechanical system

Thus, the dynamic nonlinear model of the j^{th} electromechanical system of the mobile robot is the following:

$$\begin{cases} L_j.\frac{d}{dt}\left(i_j\right) = U_{0_j} - R_{e_j}.i_j - k_{e_j}.\dot{\theta}_{e_j} \\ J_{e_j}.\frac{d}{dt}\left(\dot{\theta}_{e_j}\right) = -f_{e_j}.\dot{\theta}_{e_j} + U_j - w_j - K_j.\left(\theta_{e_j} - N_j.\theta_{s_j}\right) \\ J_{s_j}.\frac{d}{dt}\left(\dot{\theta}_{s_j}\right) = -f_{s_j}.\dot{\theta}_{s_j} + N_j.w_j + N_j.K_j.\left(\theta_{e_j} - N_j.\theta_{s_j}\right) - R.F_{x_j} \end{cases} \tag{10}$$

2.5. Robot chassis modelling

2.5.1. Kinematic Model

Fig. 1-(b) shows the robot centre of mass $G(x_G, y_G, \alpha)$, where (x_G, y_G) are the absolute coordinates and α the yaw angle. When the static radius of the robot wheel is R and the measured wheel velocities $\dot{\theta}_{s_1}$ and $\dot{\theta}_{s_2}$, then the deduced kinematic model of the robot is given as follows:

$$\begin{pmatrix} \dot{u} \\ \dot{v} \\ \dot{\alpha} \end{pmatrix} = \begin{pmatrix} R/2 & R/2 \\ R.r_1/d & -R.r_1/d \\ R/d & -R/d \end{pmatrix} . \begin{pmatrix} \dot{\theta}_{s_1} \\ \dot{\theta}_{s_2} \end{pmatrix} \tag{11}$$

with: $\dot{u}$ the longitudinal velocity of the centre of mass, $\dot{v}$ the lateral velocity of the centre of mass, $\dot{\alpha}$ the yaw velocity, d the normal distance between the wheels and $r_1$the distance between the wheel axis and the centre of the mass.

2.5.2. Geometric Model

These model concerns the deduction of the (x_G, y_G) coordinates at the absolute reference (Fig. 1-(b)). Thus, from equations (11) and after geometrical projection, this following system of equations is obtained:

$$\begin{cases} x_G = \int (\dot{u}.\cos\alpha - \dot{v}.\sin\alpha)\,.dt + x_{G_0} \\ y_G = \int (\dot{u}.\sin\alpha + \dot{v}.\cos\alpha)\,.dt + y_{G_0} \end{cases} \tag{12}$$

where: (x_{G_0}, y_{G_0}) are deduced from initial conditions.

2.5.3. Dynamic Model of the robot

This model regroups the longitudinal and yaw dynamics, where the input sources considered in our case are Fx_1 and Fx_2 (Fig. 1-(b)). These efforts are supposed known and equal to a necessary effort to tract the system, in our case they are identified as a *Coulomb* effort. Then, the only the viscous friction is considered as a reaction contact effort, due to the small dimension of the contact area. The following dynamics are synthesized from bond graph representation:

- Longitudinal dynamic: From Fig. 1-(b), the following bond graph model (Fig. 10) is synthesized:

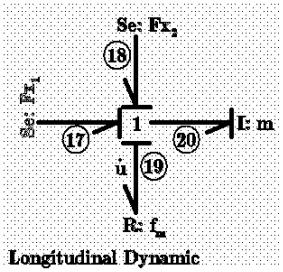

Figure 11: longitudinal dynamic of the robot

Let's note e_{20}, P_{20}, M_{20} effort, momentum and algebraic value of element I of Fig. 10, f_{19} is the flow variable of link 19, then the following state equation (13) is obtained:

$$e_{20} = -f_m.\frac{P_{20}}{M_{20}} + Se_{17} + Se_{18} \tag{13}$$

with:

$$\begin{cases} f_{17} = f_{18} = f_{19} = f_{20} = \dot{u} \\ Se_{17} = F_{x_1} \\ Se_{18} = F_{x_2} \end{cases}$$

Dynamic longitudinal equation is given in equation (14), where the longitudinal velocity $\dot{u}$ is in function of the measured angular wheel velocities, according to the kinematic model (11):

$$F_{x_1} + F_{x_2} - f_m.\dot{u} = m.\ddot{u} \tag{14}$$

- Yaw dynamic: From Fig. 1-(b), the following bond graph model (Fig. 12) is synthesized:

  Let's note e_{26}, P_{26}, M_{26} effort, momentum and algebraic value of element I of Fig. 12, then the following state equation (15) is obtained:

$$e_{26} = -f_z.\frac{P_{26}}{M_{26}} + e_{22} + e_{24} \tag{15}$$

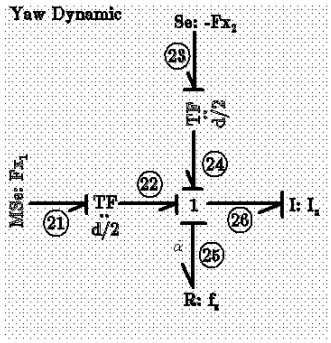

Figure 12: Yaw dynamic bond graph model of the robot in integral causality

with:

$$\begin{cases} f_{22} = f_{24} = f_{25} = f_{26} = \frac{P_{26}}{M_{26}} = \dot{\alpha} \\ e_{22} = \frac{d}{2}.F_{x_1} \\ e_{24} = \frac{d}{2}.F_{x_2} \end{cases}$$

Dynamic yaw equation is given in equation (16), where the longitudinal velocity $\dot{\alpha}$ is in function of the measured angular wheel velocities, according to the kinematic model (11):

$$(F_{x_1} - F_{x_2}) . \frac{d}{2} - f_z . \dot{\alpha} = I_z . \ddot{\alpha} \tag{16}$$

where: F_{x_1} and F_{x_2} are respectively the longitudinal efforts, f_m, f_z are the viscous friction parameters of the robot, according to longitudinal and yaw motions. d is the linear distance between the two wheels. As it is mentioned at the introduction of this section, because the longitudinal efforts are supposed known, they are taken in our case as a system inputs.

2.6. Transmission Channel Modelling

The used serial line is asynchronous with TTL levels $(0 - 5V)$. For the studied case, the serial line powers the robot and its length is limited to two meters. Concerning the modelling step, two hypothesis are assumed:

1. According to the cable length, the induced delays are neglected and the data-packet loss are not considered;

2. All external disturbances as noises or equivalent are not considered.

Several transmission channel models are proposed in the literature according to the applications requirements. Among them, in [11], an approach taking into account the resistive dissipation and based on a concatenation of basic RLC cells is presented. This approach is used for modelling our two meters length serial cable. It consists on representing the channel as a succession of symmetrical RLC cells, in order to preserve the equality of all the electrical equations for the couple (voltage, current) of each point of the channel, during the transmission time. In Fig. 13-(a), a representation on what could be the RLC cell of the length l from the channel, and Fig. 13-(b) describes an asymmetric RLC cell, where the basic two elements R_L and L_L are divided in order to create other equivalent elements. Fig. 14 shows the symmetric RLC cell of the channel with the length l.

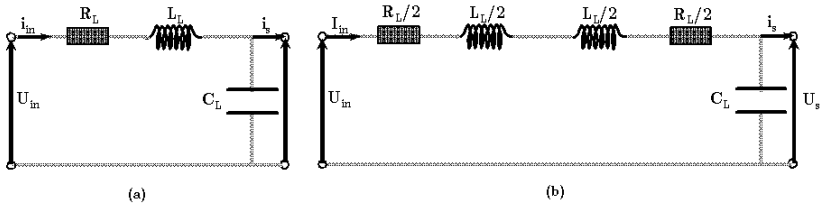

Figure 13: (a): Standard RLC circuit, (b): Asymmetric RLC cell

The studied serial cable is modelled by only one cell on the whole length. Its correspondent elements are identified experimentally.

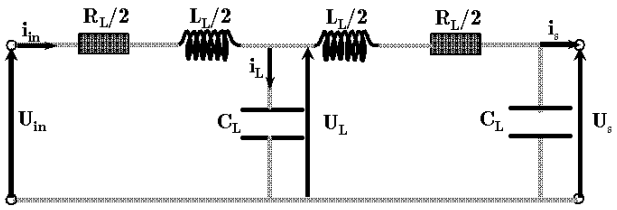

Figure 14: Symmetric RLC cell

- For the first junction 1, the effort, momentum and algebraic value of element I of Fig. 15 are noted e_{28}, P_{28}, M_{28}, then the following state equation (17)

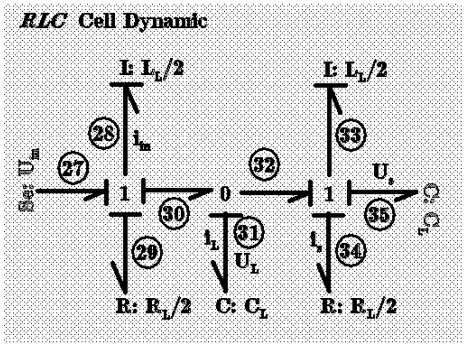

Figure 15: Bond graph model in integral causality of one cell RLC circuit of the serial transmission cable

is obtained:

$$e_{28} = -R_L.\frac{P_{28}}{M_{28}} + e_{27} - e_{30} \tag{17}$$

with:

$$\begin{cases} f_{30} = f_{29} = f_{27} = f_{28} = \frac{P_{28}}{M_{28}} = i_{in} \\ e_{27} = U_{in} \\ e_{30} = e_{31} = \frac{1}{C_L}.\int f_{31}.dt = U_L \\ f_{31} = i_L \\ f_{28} = \frac{2}{L_L}.\int e_{28}.dt \end{cases}$$

Thus, the dynamic equation issued from this junction is the following:

$$\frac{L_L}{2}.\frac{d}{dt}(i_{in}) = -\frac{R_L}{2}.i_{in} + U_{in} - U_L \tag{18}$$

- For the junction 0, the state equation deduced from the bond graph element C is given by equation (19):

$$e_{31} = -\frac{1}{C_L}.\int f_{31}.dt \tag{19}$$

with:

$$f_{31} = f_{30} - f_{32} = i_{in} - i_s$$

Thus, the dynamic equation issued from this junction is the following:

$$C_L.\dot{U}_L = i_{in} - i_s \tag{20}$$

- For the second junction 1, the effort, momentum and algebraic value of element I of Fig. 15 are noted e_{33}, P_{33}, M_{33}, then the following state equation (21) is obtained:

$$e_{33} = -\frac{R_L}{2}.\frac{P_{33}}{M_{33}} + e_{32} - e_{35} \tag{21}$$

with:

$$\begin{cases} f_{32} = f_{33} = f_{34} = f_{35} = \frac{P_{33}}{M_{33}} = i_s \\ e_{35} = \frac{1}{C_L}.\int f_{35}.dt = U_s \\ e_{32} = e_{30} = \frac{1}{C_L}.\int f_{31}.dt = U_L \\ f_{33} = \frac{2}{L_L}.\int e_{33}.dt \end{cases}$$

Thus, the dynamic equation issued from this junction is the following:

$$\frac{L_L}{2}.\frac{d}{dt}(i_s) = -\frac{R_L}{2}.i_s + U_L - U_s \tag{22}$$

Comparing the obtained dynamic equations with those issued from the $Kirchoff$ law, applied on Fig. 14, the following system can be obtained:

$$\begin{cases} \frac{L_L}{2}.\frac{d}{dt}(i_{in}) = -\frac{R_L}{2}.i_{in} + U_{in} - U_L \\ C_L.\dot{U}_L = i_{in} - i_s \\ \frac{L_L}{2}.\frac{d}{dt}(i_s) = -\frac{R_L}{2}.i_s + U_L - U_s \end{cases} \tag{23}$$

with: R_L, L_L and C_L are respectively the resistance, inductance and the capacity of the cable of length l and they are estimated experimentally according to the cable characteristics. U_{in}, U_s are respectively the known input and output cable voltages.

3. Fault Detection and Isolation Algorithm

In this section, a model based Fault Detection & Isolation algorithm (FDI) [10], [4] is build, in order to detect the transmission channel and actuators fault on the mobile robot system. This detection can help on improving the system performances from a distance.

By using the FDI algorithms proposed in [1], a list of Analytical Redundancy Relation (ARR) along with the corresponding Fault Signature Matrix (FSM) can be generated. These tools allow to detect and isolate the possible faults present on the physical system.

The FDI proposed approach is based on the calculation of the residuals issued from the Analytical Redundancy Relation (ARR) and it makes the difference between the dynamic system in normal and faulty situations. Note that for an observable system, with none unresolved algebraic loops, the number of ARR generated is equal to the number of the measured states [8]. In the studied case, the measured states are the two angular velocities of the wheel and the voltage at the end side of the transmission cable.

The main steps to generate the list of ARR and the FSM by using are summarized bellow [1]:

- Build the bond graph model in preferred integral causality;
- Put the bond graph model in preferred derivative causality after dualization of the sensors;
- Write the constitutive relation for each junction;
- Eliminate the unknown variables from each constitutive relation by covering the causal paths in the bond graph model;
- Generate the list of ARR and the corresponding FSM.

Note that for an observable system, the number of ARR generated are equal to the number of detectors on the bond graph model [1].

The first ARR_j corresponds to those generated from the j^{th} electromechanical system where its bond graph model in derivative causality. In this model, the C element is already in integral causality, because the system is sub-determined with the actual configuration. Two structurally independent ARR_j of the j^{th}

electromechanical system can be generated after eliminating the unknown variables. This elimination process is achieved by following the causal paths from unknown to known variables on the bond graph model. The secfirstond residual r_{1_j} is given as follows:

$$\begin{array}{l} r_{1_j} = k_{e_j}.\dot{\theta}_{e_j} - U_{0_j} + \frac{R_{e_j}}{k_{e_j}}.\left(J_{e_j}.\frac{d}{dt}\left(\dot{\theta}_{e_j}\right) - w_j + f_{e_j}.\dot{\theta}_{e_j}\right. \\ \left. +\frac{1}{N_j}\left(f_{s_j}.\dot{\theta}_{s_j} - N_j.w_j + J_{s_j}.\frac{d}{dt}\left(\dot{\theta}_{s_j}\right)\right)\right) + \frac{L_j}{k_{e_j}}.\frac{d}{dt}\left(J_{e_j}.\frac{d}{dt}\left(\dot{\theta}_{e_j}\right)\right. \\ \left. -w_j + f_{e_j}.\dot{\theta}_{e_j} + \frac{1}{N_j}\left(f_{s_j}.\dot{\theta}_{s_j} - N_j.w_j + J_{s_j}.\frac{d}{dt}\left(\dot{\theta}_{s_j}\right)\right)\right) \end{array} \quad (24)$$

The second residual r_{2_j} is then deduced and expressed as follows:

$$r_{2_j} = N_j.\frac{d}{dt}\left(f_{s_j}.\dot{\theta}_{s_j} + J_{s_j}.\frac{d\left(\dot{\theta}_{s_j}\right)}{dt} - N_j.w_j + R.F_{x_j}\right) + K_j.\left(N_j.\dot{\theta}_{s_j} - \dot{\theta}_{e_j}\right) \quad (25)$$

- F_{x_j} is considered as a known external forces. Finally, the corresponding residuals r_3 issued from the transmission cable is given in equation (26)

$$r_3 = U_{in} - \frac{L_L^2.C_L^2}{4}.\frac{d^4}{dt^4}\left(U_s\right) + \left(\frac{R_L^2.C_L^2}{4} - \frac{L_L.C_L}{2}\right).\frac{d^2}{dt^2}\left(U_s\right) + \frac{R_L.C_L}{2}.\frac{d}{dt}\left(U_s\right) + U_s \quad (26)$$

4. Simulation & Experimental Results

Simulation parameters used for the robot system are given in table (1). Actuators and cable parameters are given by their notice characteristics, then all the other resistances are identified experimentally. Due to the small values of the parameters, their parameter uncertainties and the models uncertainties are neglected. In order to simulate really a cable fault, a potentiometer of value $R_0 = 100\,(\Omega)$ is connected to the serial cable, in order to vary locally its resistance value. Thus, we can simulate a cut in the cable by increasing the resistance value of R_L, through R_0. The backlash dead zone $\tau_{0_j} = 0.01rad$, identified in [?] and has a neglected effect in the following experimental application.

The whole outputs are exploited by the virtual simulator bloc in order to reconstruct the robot trajectory according to the Cartesian coordinates of the

Param.	Value	Param.	Value
J_{e_1}, J_{e_2}	$0.14 \times 10^{-7}\left(kg.m^2\right)$	L_1, L_2	$300 \times 10^{-6}(H)$
f_{e_1}, f_{e_2}	$1.19\times\ 10^{-5}\left(\frac{N.m.s}{rad}\right)$	K_{e_1}, K_{e_2}	$3.51 \times 10^{-3}(\frac{N.m}{A})$
J_{s_1}, J_{s_2}	$0.1\left(kg.m^2\right)$	f_m	$0.0001\left(\frac{N.m.s}{rad}\right)$
f_{s_1}, f_{s_2}	$0.0003\left(\frac{N.m.s}{rad}\right)$	f_z	$0.0005\left(\frac{N.m.s}{rad}\right)$
R	$0.005(m)$	r_1	$0.01(m)$
d	$0.04\,(m)$	I_z	$0.0058(kg.m^2)$
R_L	$3.2(\Omega)$	m	$0.250(kg)$
C_L	$110\times\ 10^{-12}(F)$	L_L	$250 \times 10^{-9}(H)$
R_{e_1}, R_{e_2}	$17.6(\Omega)$	N_1, N_2	25

Table 1: Simulation model parameters.

robot. This virtual simulator was built by *Virtual Reality Matlab toolbox* using the model developed above. The residuals indicate the influence of the studied faults on the global system performances. In the following graphics, we show the time evolution of the residuals in normal situation Fig. 16 (*i.e. without faults*) and in faulty situations Fig. 18. The convergence of the residuals to zero indicates that the global system is in normal situation and the followed trajectory is given in Fig. 17. Fig. 19 shows the influence of the introduced fault on the system performance. However, by introducing a cable fault of Fig. 21, we can notice that only residual r_3 is sensible to this fault due to the cable fault Fig. 20, because all the regulations are made locally to the robot system and only the input system data are forwarded by the serial cable.

5. Conclusion

In this paper, a model based fault detection and isolation applied on a mobile robot with transmission channel is presented. In this case, the transmission channel is considered as a complete and separate system from the robot, and the synthesized residuals show the isolability of the cable fault from the actuators faults as shown by the simulation and the experimental results. The use of a virtual simulator developed in this framework, demonstrates the principal role of this tool to help the system supervisor in predicting and/or detecting some major faults, which can be resolved according to the state of the situation by maintenance or control reconfiguration.

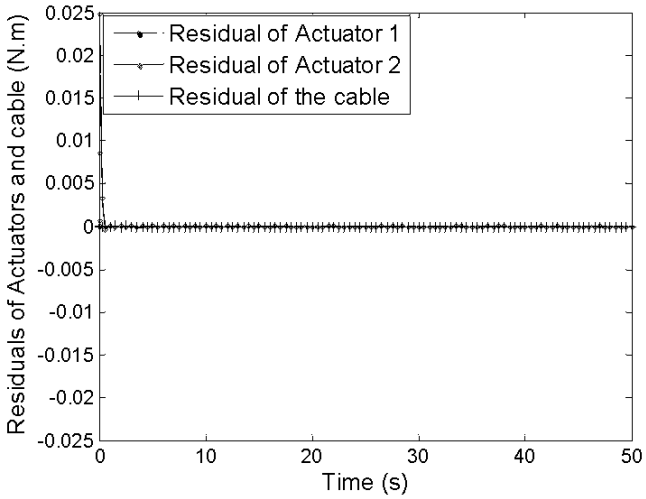

Figure 16: Residuals r_{1_2}, r_{2_2} and r_3 in normal situation

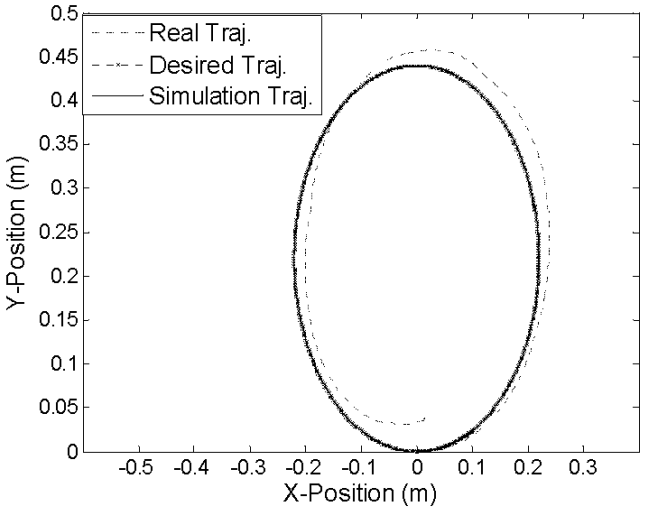

Figure 17: Desired, simulated and real robot trajectories in normal situation

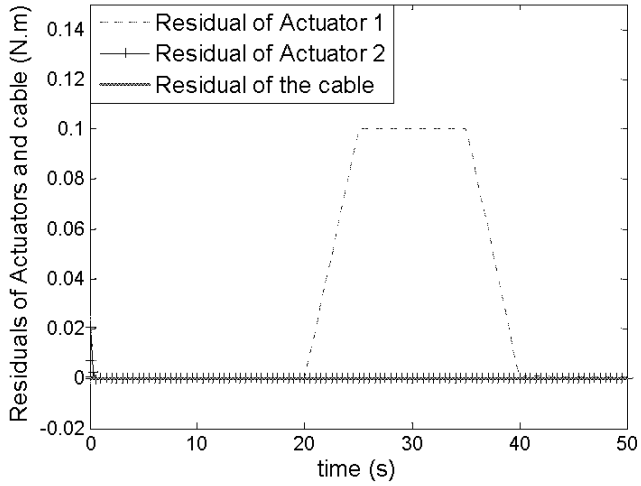

Figure 18: Residuals r_{1_2}, r_{2_2} and r_3 in actuator fault situation

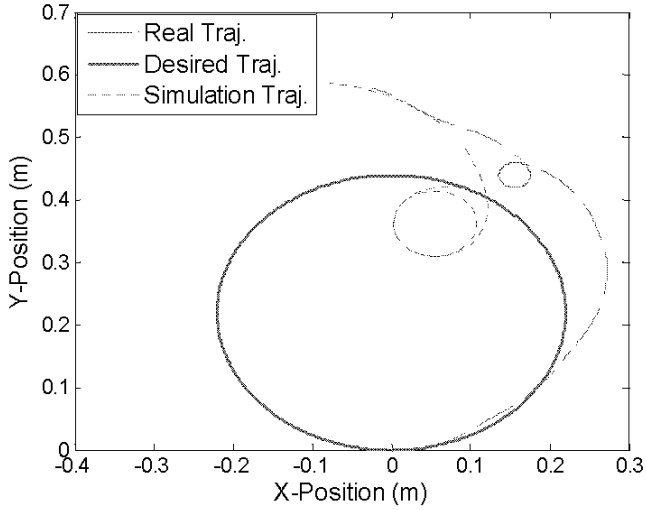

Figure 19: Desired, simulated and real robot trajectories in faulty situation

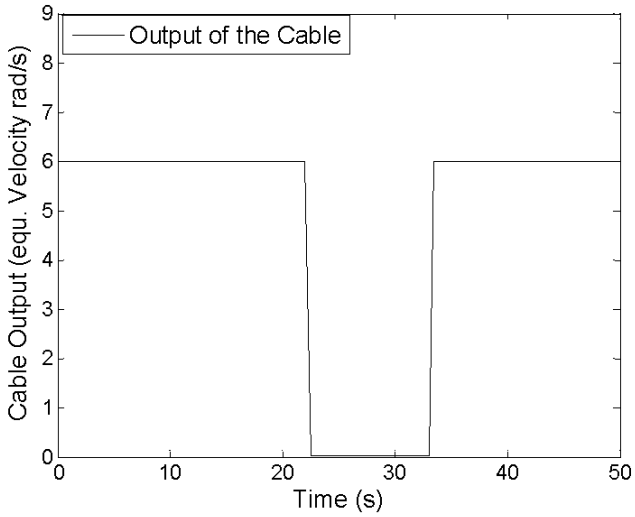

Figure 20: Fault profile on the output signal of the cable

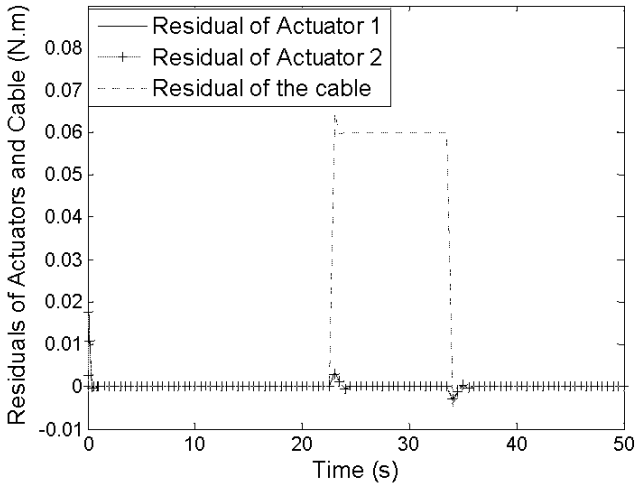

Figure 21: Residuals r_{1_2}, r_{2_2} and r_3 in transmission fault situation

References

[1] B. Ould Bouamama, A. K. Samantaray, M. Staroswiecki, and G. Dauphin-Tanguy, 'Derivation of constraint relations from bond graph models for fault detection and isolation', International Conference on Bond Graph Modeling and Simulation (ICBGM'03), pages 104-109. Simulation Series Vol.35, No.2, ISBN 1-56555-257-1, 2003.

[2] M. A. Djeziri, R. Merzouki, B. Ould-Bouamama, G. Dauphin-Tanguy, 'Bond Graph Model Based For Robust Fault Diagnosis', ACC'2007, American Control Conference, pp. 3017 - 3022, New York, USA, 2007.

[3] K-Team web site: www.k-team.com.

[4] R. Isermann, 'Supervision, fault detection and fault diagnosis methods - an introduction'. Control Engineering Practice, Vol. 5, No. 5:639—652, 1997.

[5] D. C. Karnopp, D. Margolis and R. Rosenberg, 'Systems Dynamics: A Unified approach', John Wiley, New York, second edition, 1990.

[6] D. C. Karnopp, 'An approach to derivative causality in bond graph models of mechanical systems', Journal of the Franklin Institute, Vol. 329, Issue 1, pp. 65-75, 1992.

[7] J. F. Magni and P. Mouyon, 'On residual generation by observer and parity space approaches', IEEE Trans. Autom. Control, vol. 39, no. 2, pp. 441–447, Feb. 1994.

[8] R. Merzouki, K. Medjaher, M. A. Djeziri, B. Ould-Bouamama, 'Backlash Fault Detection in Mechatronics System', MECHATRONICS IFAC Journal, Vol. 17, pp. 299-310, 2007.

[9] R. Merzouki, J.C. Cadiou, 'Estimation of Backlash Phenomenon in the Electromechanical Actuator', Journal of Control Engineering practice, Vol 13/8 pp 973-983, 2005.

[10] M. Staroswiecki and G. Comtet-Varga. Analytical redundancy relations for fault detection and isolation in algebraic dynamic systems. Automatica, Vol. 37, pp. 687—699, 2001.

[11] L. Teppoz, 'Commande d'un système de conversion de type VSC-HVDC. Stabilité-contrôle des perturbations', PhD thesis, INPG, Grenoble, France, 2005.

[12] Y. Zheng, H. Fang, and H. O. Wang, 'Takagi–Sugeno Fuzzy-Model-Based Fault Detection for Networked Control Systems with Markov Delays', IEEE Trans. On Sys., Man, and Cyb.—Part B: CYBERNETICS, Vol. 36, N°. 4, pp. 924-929, Aug 2006.

[13] Y. Zheng, H. Fang, and Y. Wang 'Kalman Filter Based FDI of Networked Control System', Proceedings of the 5m World Congress on Intelligent Control and Automation, Hangzhou, pp. 1330-1333, P. R. China.2, 2004.

[14] H. Ye, G. Wang, and S. X. Ding 'A New Parity Space Approach for Fault Detection Based on Stationary Wavelet Transform', IEEE Transaction on Automatic Control., Vol. 49, N°. 2, pp. 281-287, Feb 2004.